energy&fuels

pubs.acs.org/EF Article

Reaction Mechanisms of Anisole Pyrolysis at Different Temperatures: Experimental and Theoretical Studies

Ting Zhang, Chiranjivi Bhattarai, Yeongkwon Son, Vera Samburova, Andrey Khlystov,* and Sergey A. Varganov*

Cite This: *Energy Fuels* 2021, 35, 9994−10008 Read Online

ACCESS | Metrics & More | Article Recommendations | Supporting Information

ABSTRACT: Pyrolysis of tar compounds plays an important role in designing optimal thermochemical processes for the conversion of biomass into globally important commodities. Therefore, it is crucial to understand the relevant reaction mechanisms and be able to predict the decomposition products of these compounds at different temperatures. In this study, the pyrolysis of anisole, which serves as an important model compound for lignin, a major component of biomass tar, was studied in a laminar-flow reactor system of N_2 gas at temperatures of 300−650 °C and a residence time of 1 s. The decomposition products were analyzed using a gas chromatograph with mass spectrometric and flame ionization detectors. To gain insights into the reaction mechanisms, detailed studies of the unimolecular and bimolecular decomposition pathways were carried out using the density functional theory and high-level coupled cluster methods. Anisole was found to decompose at temperature as low as 400 °C, which is the lowest reported temperature for anisole decomposition. Formation of benzene and toluene at low temperatures (400−450 °C) is explained by the low-energy barrier ipso-addition of CH_3 and H radicals at the methoxy moiety of anisole. At 500−550 °C, multiple reaction mechanisms lead to the formation of benzofuran, methylcyclopentadiene, benzaldehyde, cyclopentadiene, ethylbenzene, styrene, and *o*-xylene. Finally, at 600−650 °C, indene, phenol, and cresol were detected. The obtained results are expected to contribute to the development of predictive kinetic models for the decomposition of anisole and other similar compounds.

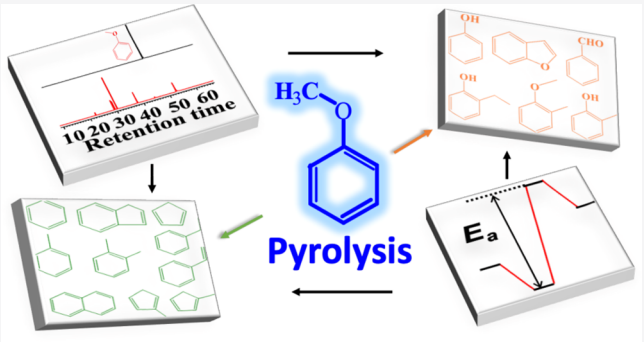

1. INTRODUCTION

Biomass, such as lignin, hemicellulose, and cellulose,[1] represents an alternative energy source. In the future, biomass pyrolysis is expected to become one of the promising technologies contributing to the partial replacement of non-renewable fossil fuels.[2−5] Because lignin is an inexpensive and abundant biomass,[6,7] its conversion to globally important commodities has attracted a lot of attention. Anisole, as the simplest aromatic model compound for the methoxy group in lignin, is not only a significant component in biomass pyrolysis oils[8] but also has outstanding combustion properties.[9,10] Thus, to define optimal operating conditions for lignin conversion, anisole is commonly selected as a potential surrogate compound to mimic lignin pyrolysis and combustion.[11,12] Because the O−CH_3 bond is significantly weaker than other bonds in anisole, studying the anisole decomposition can provide valuable insights into the chemistry of phenoxy and cyclopentadienyl, which are important intermediates in the formation of polycyclic aromatic hydrocarbons and soot during biomass pyrolysis and combustion.[13] In addition, as anisole has become popular as a fluorescence tracer,[14−16] the study of its thermal decomposition could help us to access the temperature and time range where it can be used in fluorescence spectroscopy.[17] Anisole and its pyrolysis are also relevant for the food industry[18−20] and public health policies related to the flavor use in tobacco and electronic cigarette products.[21−23]

To date, multiple studies of anisole reactivity, pyrolysis, oxidation, and combustion have been conducted with well-controlled experimental conditions, various state-of-the-art detection techniques, and theoretical methods, leading to determining relevant rate constants, species concentration profiles, reaction pathways, and kinetic models. Mulcahy et al.[24] reported that H-abstraction on the methoxy group of anisole by a methyl radical is much faster than that on the aromatic ring at 487 K. Paul and Back[25] first measured the C−O bond dissociation energy (238.5 kJ/mol) in the methoxy group of anisole in a glass vacuum apparatus. Schlosberg et

Received: March 20, 2021
Revised: May 10, 2021
Published: May 25, 2021

https://doi.org/10.1021/acs.energyfuels.1c00858
Energy Fuels 2021, 35, 9994−10008

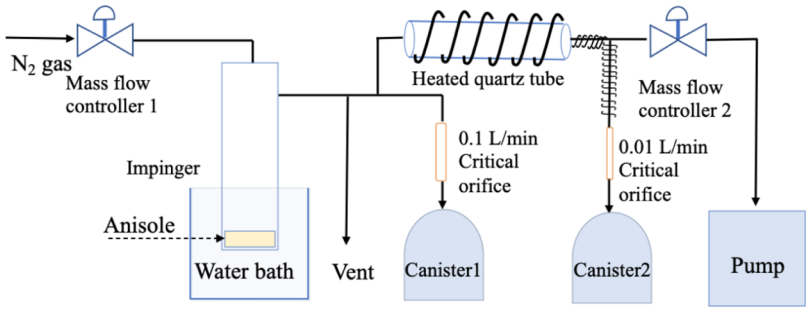

Figure 1. Block-flow diagram of the pyrolysis reaction system.

al.[26] studied pyrolysis of anisole in an autoclave and detected different main products at low and high temperatures. Later, research efforts were focused on understanding the initial unimolecular decomposition in pyrolysis of anisole, which proceeds via homolytic dissociation to form phenoxy and methyl (CH_3) radicals and is consistent with the higher bond energy of CH_2-H than that of $C_6H_5O-CH_3$. The reaction rate constants were measured at low to atmospheric pressures in a shock tube,[27] a stirred reactor,[28,29] and a flow reactor in the presence of hydrogen.[30] At the same time, the rate constant of the further decomposition of the phenoxy radical to form cyclopentadienyl (C_5H_5) and CO was also measured[17,27,31,32] and supported with a theoretically proposed mechanism[33−35] involving formation of a bicyclic intermediate and ring opening. CH_3, C_5H_5, and phenoxy radicals, which were found to be important intermediates, can recombine with an H radical or with themselves, leading to many different products. These include light compounds, such as CH_4 and C_2H_6, and heavier products, such as cyclopentadiene, methylcyclopentadiene, phenol, naphthalene, benzene, and cresol.[13,30,36−42] Anisole can also participate in the bimolecular reaction with H and CH_3 radicals, forming benzene, toluene, and benzaldehyde at low temperature.[13,41,43] Pecullan et al.[36] studied the first step of anisole oxidation in an atmospheric pressure flow reactor, showing that the differences between the types of pyrolysis and oxidation products are small. Nowakowska et al.[41] and Wagnon et al.[1] further studied anisole oxidation in a jet-stirred reactor and developed a more complex mechanism of anisole pyrolysis. With these speciation measurements, detailed and comprehensive kinetic models for anisole pyrolysis and oxidation were developed by several groups using various reactors and detectors,[13,30,36,38,41,42,44,45] proposing different reaction mechanisms at low and high temperatures.

Recently, to better understand the behavior of anisole during realistic combustion scenarios, the effects of combustion parameters, such as ignition delay times,[46,47] laminar flame speeds,[1,48] and the chemical structure of laminar premixed flames of anisole,[49] were investigated. Furthermore, Ranzi and co-workers[50] presented a kinetic model[51] systematically describing the pyrolysis and combustion of anisole and other substituted phenolic species from bio-oils, focusing on defining reaction classes and rate rules. While these studies showed that reaction mechanisms of anisole pyrolysis are very complex, efforts were focused more on experimental characterization of the decomposition products than on elucidation of the reaction mechanisms, especially for those products with multiple formation pathways. Although multiple species and reactions were considered in the kinetic models, several recent models were shown to either overestimate or underestimate experimental yields for different products,[36,41,42] indicating that a better understanding of the reaction mechanisms is needed. Despite a detailed mechanistic study of several unimolecular and recombination reactions of anisole pyrolysis by Koirala[42] and a comprehensive kinetic model of the pyrolysis and combustion of anisole by Ranzi and co-workers,[50] there are still significant knowledge gaps in our understanding of the corresponding reaction networks.

To fill these knowledge gaps, in this work, anisole pyrolysis was studied in a laminar flow of N_2 gas at a temperature of 300−650 °C and 1 atm pressure with a residence time of 1 s. The decomposition products were analyzed with a gas chromatography instrument coupled with mass spectrometry and flame ionization detectors (GC−MS/FID). Then, detailed mechanistic studies using the density functional theory (DFT) and high-level coupled cluster methods were carried out to probe possible unimolecular and biomolecular pathways responsible for the formation of experimentally identified products. The predicted energies of the transition states (TSs) and intermediates along different reaction pathways were used to identify the dominant reaction mechanisms at different temperatures.

2. METHODS

2.1. Experimental Methods. Anisole thermal pyrolysis experiments were performed in an apparatus outlined in Figure 1, in which the reactor system is similar to that discussed elsewhere.[42,52,53] First, to evaporate a small amount of anisole, a glass impinger was filled with anisole (>99%, Fisher Scientific International, Inc. Ottawa, Ontario, Canada) and kept at a constant temperature of 21 °C (room temperature) in a water bath. At the same time, N_2 gas (99.9% high purity, Airgas, Inc., Radnor, PA, USA) at 200 mL/min (controlled using a mass flow controller at room temperature and atmospheric pressure) was continuously dispersed into the vaporizer, carrying anisole into three places: (a) a heated reactor for decomposition reactions, (b) directly into a Summa canister (model X56L, 6L, Meriter, San Jose, CA, USA) for measurements of the anisole concentration before decomposition, and (b) into a vent for remaining gas release. Canister sampling was performed at a flow rate of 100 mL/min using a critical orifice (O'Keefe Controls Co., Monroe, CT, USA). Canisters were cleaned prior to sampling by repeated evacuation and pressurization with humidified zero air according to the procedure described in a previous study.[54]

The reactor is a quartz tube of 4 mm inner diameter, 6 mm outer diameter, and 270 mm heated length. It is heated using an insulated heating tape (BriskHeat Corporation, Columbus, OH, USA) controlled at a set point temperature using a proportional-integral-derivative (PID) controller (Omega Engineering Inc., Norwalk, CT, USA) and insulated with a glass wool. Prior to the experiments, the reactor temperature was calibrated by measuring gas temperature along the reactor axis with a J-type thermocouple. The centerline temperature profiles in the reactor at set points in the range of 400−

https://doi.org/10.1021/acs.energyfuels.1c00858
Energy Fuels 2021, 35, 9994−10008

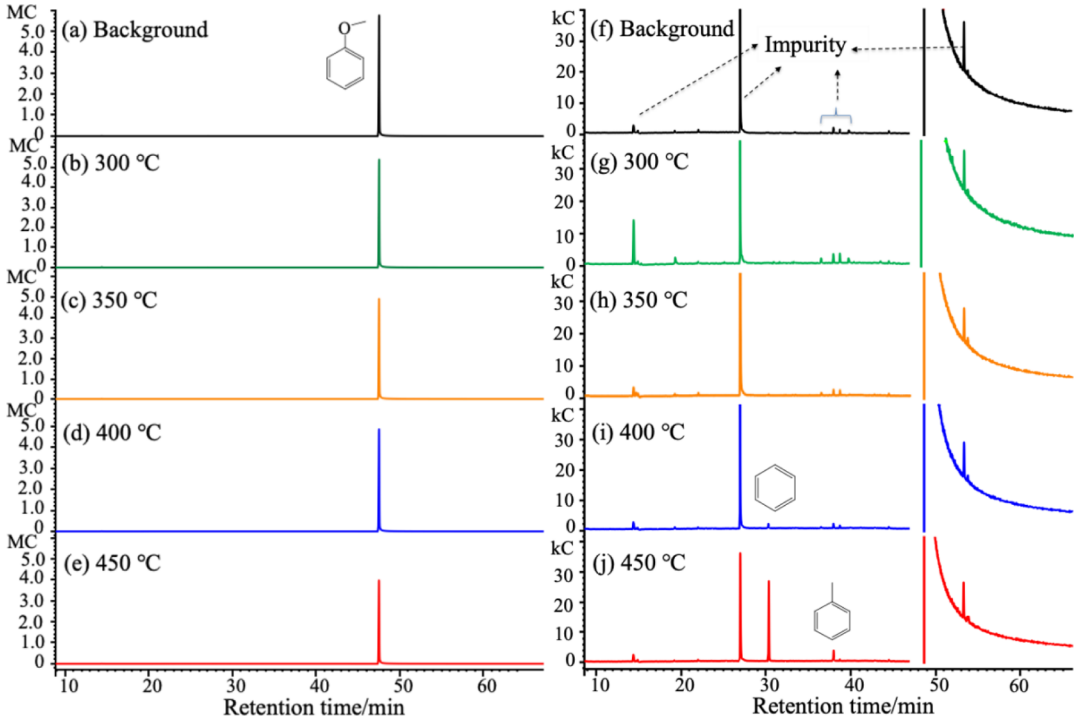

Figure 2. GC−MS chromatograms of anisole decomposition products at 300−450 °C. The vertical axis shows the total ion count. Chromatograms of the same color show the same samples analyzed using different injections: 5 mL (a−e) and 300 mL (f−i). Note that the acquisition was stopped between 47 and 49 min retention time to protect the MS filament (f−j) due to the very strong intensity of the anisole signal that elutes at this time. There are traces of impurity in anisole, marked in panel (f).

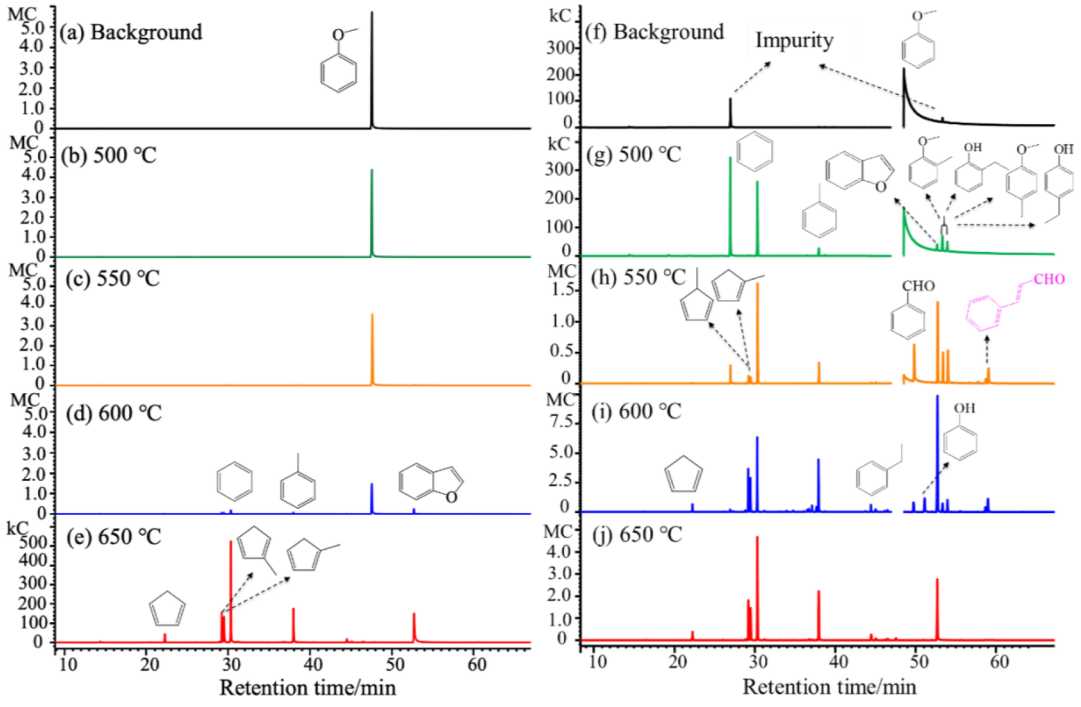

Figure 3. GC−MS chromatograms of anisole decomposition products at 500−650 °C. The vertical axis shows the total ion count. Chromatograms of the same color show the same samples analyzed using different injections: 5 mL (a−e), 300 mL (f−i), and 50 mL (j). Note that the acquisition was stopped between 47 and 49 min retention time to protect the MS filament (f−i) due to the very strong intensity of the anisole signal that elutes at this time. There are traces of impurity in anisole, marked in panel (f). Compounds marked pink are assigned based on the NIST mass spectral database.

750 °C in 50 °C increments are shown in Figure S1. The centerline temperature increases from a value of 200−350 °C lower than the set point in the first 75 mm, keeps steady with a value of about 10 °C higher than the set value in the midpart of about 125 mm, and finally decreases by 300−500 °C in the last 70 mm part of the tube, which is similar to that in other reactors reported in previous studies.[42,52] The

https://doi.org/10.1021/acs.energyfuels.1c00858
Energy Fuels 2021, 35, 9994−10008

midpart of the tube with a steady temperature was selected as the effective reaction segment. Anisole decomposition was carried out in the flow reactor at set temperatures ranging from 300 to 650 °C in 50 °C increments. The residence time in the reaction segment was kept at 1 s, which is defined by dividing the midpart volume by the gas flow rate adjusted for the temperature in the reactor. These operating parameters are relevant to those found in industrial pyrolysis and combustion processes.[2,53] Upon exiting the reactor, a part of the gas steam containing the products and unconverted anisole was sampled with a canister through a critical orifice (with a flow rate of 10 mL/min), while the remaining flow (between 25 and 40 mL/min) from the reactor was drawn using a pump. The lines after the reactor and before the canister were heated using heating tapes to about 180 °C to prevent condensation of heavy reaction products.

Prior to GC−MS/FID analysis, the sampled canisters were pressurized with high-purity N_2 gas. The GC−MS/FID system consisted of a Lotus Consulting Ultra-Trace Toxics sample preconcentration system built into a Varian 3800 GC coupled with a Varian Saturn 2000 ion trap mass spectrometer and flame ionization detector. Varian MS Workstation Version 6.9 software was used for data processing. A detailed description of the system is presented elsewhere.[54] Light species (including those with less than six carbon atoms) were separated on a Varian CP-Sil5 column (15 m × 0.32 mm × 1 μm) and a Chrompack Al_2O_3/KCl column (25 m × 0.53 mm × 10 μm) and quantified with an FID detector. Heavier species were separated on a J&W DB-1 column (60 m × 0.32 mm × 1 μm) connected to the ion trap mass spectrometer. Products are identified by matching the mass spectrum of each product with the mass spectrum of a compound in the National Institute of Standard and Technology (NIST) mass spectral library database, (NIST MS Research 2.0). Some hydrocarbon products (Table S1) are further identified by comparing the retention time and mass spectrum of each product with those of the corresponding reference standard compound in the calibration gas mixture of 75 hydrocarbon compounds from ethane to *n*-undecane (Apel-Reimer Environmental Inc., Broomfield, CO, USA).[54] The statistical uncertainty of the measurements was investigated by observing variations in peak intensity during four repeated experiments and three repeated GC−MS/FID measurements of the same sample. The overall uncertainty was found to be less than 8%.

2.2. Computational Methods. Molecular geometries of reactants, products, intermediates (Is), and TSs were optimized with the DFT method using the M06-2X[55] functional in combination with the def2-TZVP[56] basis set, which was shown to produce accurate structures and reasonable TS barriers.[57,58] Harmonic vibrational frequencies were computed at the same level of theory to ensure that the TS structures are characterized by a single imaginary frequency, while all other structures have no imaginary frequencies. Intrinsic reaction path[59] calculations were performed to connect TSs with the minima corresponding to the reactant, product, or Is. Finally, to obtain more accurate reaction barriers, energies of TSs and minima were calculated using the explicitly correlated coupled cluster F12-CCSD(T) method[60] with the same basis set. All DFT calculations were performed using the General Atomic and Molecular Electronic Structure System (GAMESS) suite of programs,[61,62] while the coupled cluster calculations were carried out with Molpro quantum chemical software.[63]

3. RESULTS AND DISCUSSION

3.1. Experimental Results. The anisole decomposition experiments were conducted in the flow reactor at a residence time of 1 s in N_2-diluted mixtures at atmospheric pressure and temperatures of 300−650 °C. GC−MS chromatograms of the products measured at these temperatures are shown in Figures 2 and 3. More details for temperatures between 500 and 650 °C are presented in Figures S2 and S3, and the appearance of each compound at different temperatures along with the confirmation confidence is listed in Table S1. Anisole was inert at low temperatures of 300 and 350 °C, as is apparent from the anisole signal remaining the same (Figure 2b,c) and the absence of new peaks in the chromatograms (Figure 2g,h). Contrary to the previously reported observations that the lowest temperature of anisole decomposition (as evidenced by benzaldehyde production) is 477 °C,[41] a small peak corresponding to benzene first appeared at 400 °C (Figure 2i), which indicates the beginning of anisole decomposition. This is the lowest reported temperature for anisole decomposition, compared with the previously reported temperatures of 477 °C[41] and 587 °C[29] in a stirred reactor and 500 °C in a flow reactor.[42] With the temperature increasing to 450 °C, more anisole was converted (Figure 2e), and formation of toluene and a larger amount of benzene was detected (Figure 2j).

When the temperature was increased to 500−650 °C (Figure 3), more anisole was consumed, and dozens of new species were produced. The amount of benzene and toluene increased significantly as temperatures increased. At 500 °C, oxygenated products, including benzofuran, *o*/*p*-methylanisole, and *o*/*p*-ethylphenol, started to appear (Figure 3g), and two isomers of methylcyclopentadiene, 1-methylcyclopentadiene, and 2-methylcyclopentadiene were also detected (Figure S2g). The last two are known as the two mixed stable isomers of methylcyclopentadiene at room temperature.[29] Similar to benzene and toluene, methylcyclopentadiene and benzofuran were formed in larger quantities as temperature increased to 650 °C. At 550 °C, three other oxygenated compounds, benzaldehyde, *o*-ethylanisole, and cinnamaldehyde (Figure 3h), were formed along with 1,3-cyclopentadiene and several aromatic compounds (Figure S2h), including ethylbenzene, styrene, and *o*/*p*-xylene. When temperature increased to 600 °C, more than 80% of anisole was consumed, and phenol was formed, with the small peaks (Figure S3i) attributed to *o*/*p*-cresol, indene, and naphthalene. At 650 °C, almost all anisole was consumed, and the amount of most hydrocarbon products and benzofuran reached the highest level. In contrast, the amount of reactive oxygenated products decreased significantly. The amount of cinnamaldehyde was reduced by about five times, and other compounds, including benzaldehyde, phenol, *o*/*p*-cresol, *o*/*p*-methylanisole, and *o*/*p*-ethylphenoxy, disappeared (Figures 3j and S3j). The intensity of the naphthalene peak decreased almost to zero because the six times lower amount of the injected anisole led to the detection difficulty. According to the NIST mass spectra database,[64] the peaks at a retention time of 53.4 and 54.0 min may represent *o*/*p*-methylanisole or *o*/*p*-ethylphenol with the same molecular weight, respectively.[42] The peaks at 57.7 and 59.0 min, tentatively assigned to *o*-ethylanisole and cinnamaldehyde, respectively, have not been reported previously. Similarly, several other peaks at 51.1, 52.0, 61.8, and 63.3 min in Figure S3 were assigned only based on the NIST database.

Apart from aromatic compounds and some five-member ring species, several light compounds and other nonaromatic decomposition products were also detected, in agreement with previous studies.[13,36,41,42] As seen in Figure S2c−e, at temperatures of 550−650 °C, there are several peaks assigned to light hydrocarbons, including propene (C_3H_6), propyne (C_3H_4), 1,3-butadiene (C_4H_6), vinylacetylene (C_4H_4), and 1,4-pentadiene (C_5H_8). Based on the FID detection (Figure S4), several other hydrocarbons were identified and quantified, including large amounts of ethane (C_2H_6) and ethene (C_2H_4), as well as a small amount of acetylene (C_2H_2), propane

https://doi.org/10.1021/acs.energyfuels.1c00858
Energy Fuels 2021, 35, 9994−10008

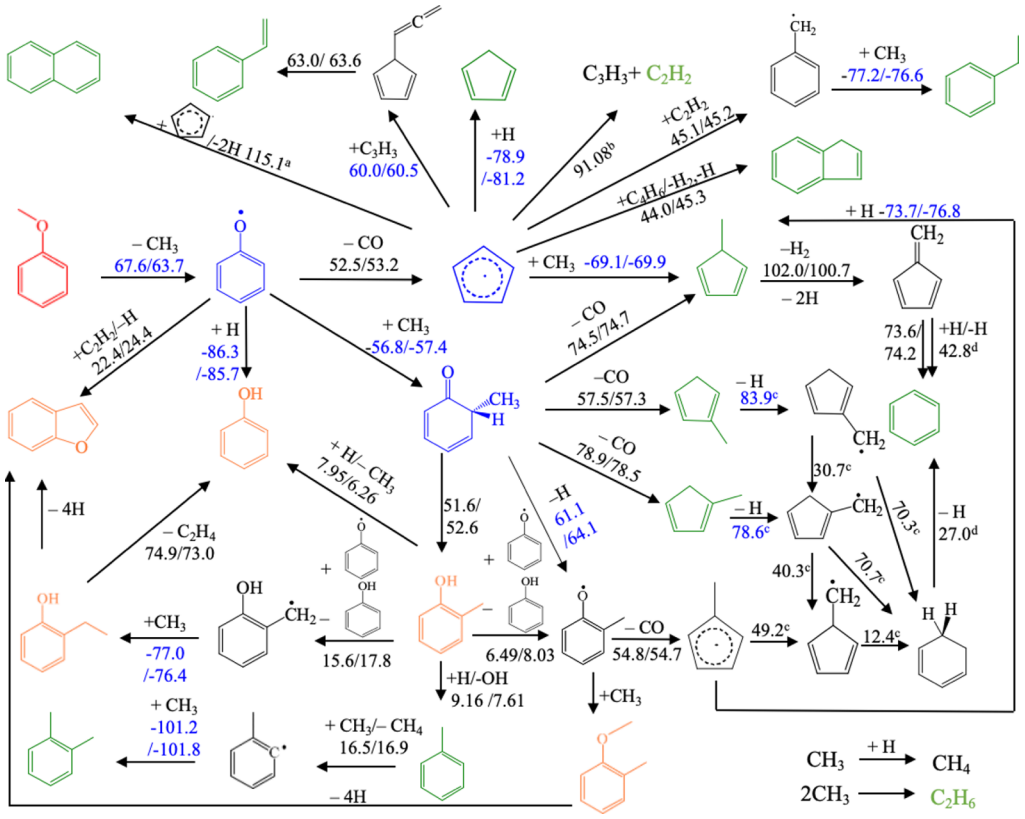

Figure 4. Reaction network of unimolecular anisole decomposition. Energies (kcal/mol) of the TSs (black) and products (blue) with respect to reactants predicted by M06-2X and F12-CCSD(T) methods are shown in the format $E_{M06\text{-}2X}/E_{F12\text{-}CCSDT(T)}$. Superscripts above the energy values are a—ref 37, b—ref 65, c—ref 66, and d—ref 67. The molecular structures are labeled as red—anisole, green—detected hydrocarbon products, orange—detected oxygenated products, blue—important intermediates, and black—other compounds.

(C_3H_8), *n*-butane (*n*-C_4H_{10}), 1-butene (1-C_4H_8), and *n*-pentane (*n*-C_5H_{12}). The amount of these hydrocarbons increased with temperature. As reported in previous studies,[13,36,41,42] other light compounds including hydrogen, carbon monoxide, and methane also should be formed during anisole decomposition. Hydrogen and methane are generated in H-abstraction reactions by H and methyl radicals, respectively.[41] Carbon monoxide can be generated in the decomposition of phenoxy, methylphenoxy, methylcyclohexadienone, and benzoyl.[13,27,29,36,41] The corresponding reaction mechanisms will be discussed in the following computational section. However, these light compounds were not analyzed in this work due to the limitation of detection methods.

3.2. Computational Results. To understand the complex reaction mechanism of anisole decomposition, DFT geometry optimizations were performed for primary reaction pathways, and the energies were refined with F12-CCSD(T). In the following discussion, we will use the more accurate F12-CCSD(T) energies. Based on previous studies,[13,36,41,42] the overall reaction network of anisole decomposition was separated into two parts, unimolecular decomposition (Figure 4) and bimolecular decomposition (Figure 5). Note that the reaction mechanisms with *para* intermediates are not displayed because they are similar to those with *ortho* intermediates.

The oxygen–carbon bond of the O–CH_3 group is the weakest bond in anisole, with the predicted bond energy of 63.7 kcal/mol, which is close to 63.2 kcal/mol reported in a recent study.[41] The unimolecular decomposition is initiated by breaking this bond, producing methyl and phenoxy radicals. Apart from the further high-temperature decomposition to

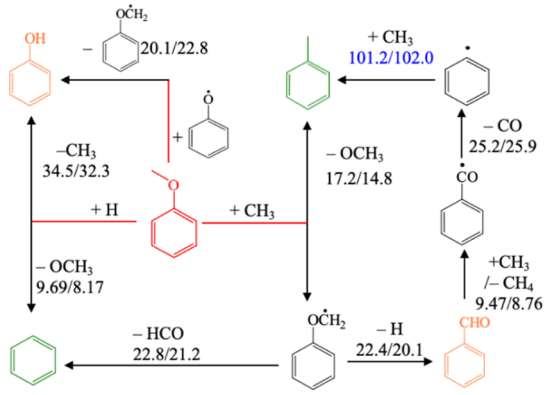

Figure 5. Reaction network for bimolecular reactions of anisole with CH_3, H, and phenoxy radicals. Energies (kcal/mol) of TSs (black) and products (blue) with respect to those of reactants predicted with M06-2X and F12-CCSD(T) are shown in the format $E_{M06\text{-}2X}/E_{F12\text{-}CCSDT(T)}$. The molecular structures are labeled as red—anisole, green—detected hydrocarbon products, orange—detected oxygenated products, and black—other compounds.

form the cyclopentadienyl radical and CO, the phenoxy radical can recombine with CH_3 to form *o*/*p*-methylcyclohexadienone. The last, along with phenoxy, methyl, and cyclopentadienyl radicals, plays an important role in producing multiple aromatic hydrocarbons and oxygenated compounds, as seen in Figure 4. The phenoxy radical also contributes to the direct formation of benzofuran and phenol. Once *o*/*p*-methylcyclohexadienone is formed, it can dissociate to three isomers of

https://doi.org/10.1021/acs.energyfuels.1c00858
Energy Fuels 2021, 35, 9994–10008

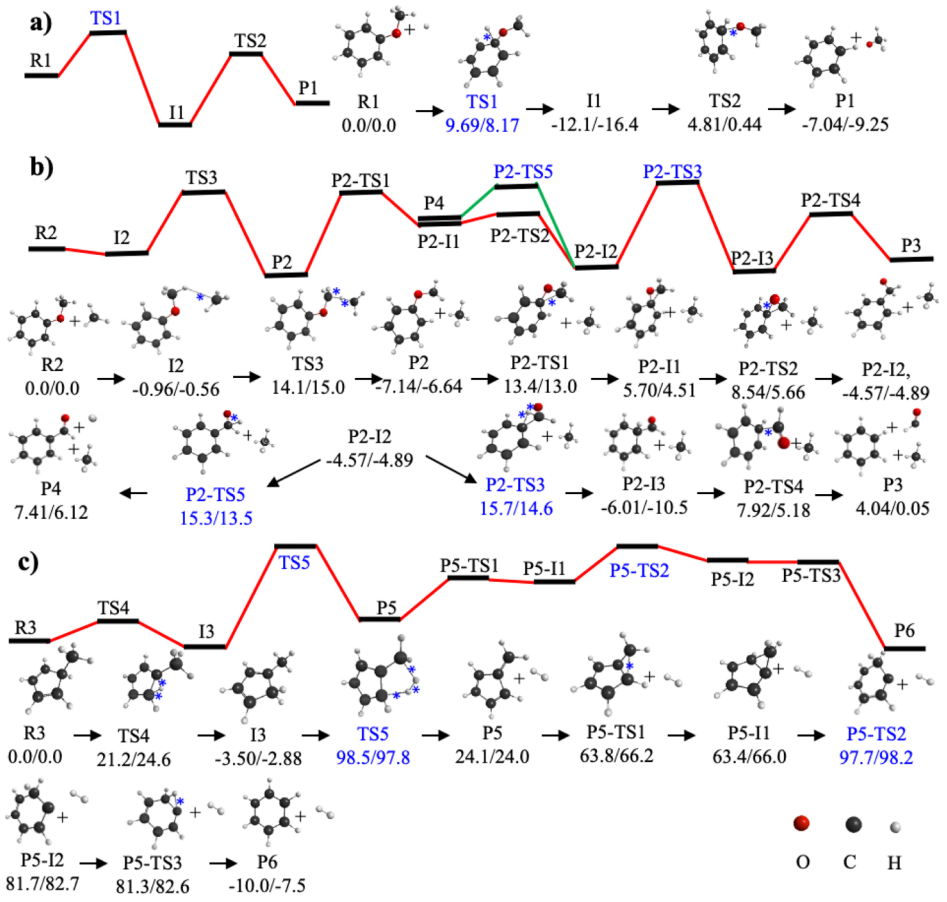

Figure 6. Reaction pathways for formation of benzene (red) and benzaldehyde (green): (a) anisole + H, (b) anisole + CH_3, and (c) dissociation of 5-methylcyclopentadiene. The energies (kcal/mol) are reported in the format $E_{M06\text{-}2X}/E_{F12\text{-}CCSDT(T)}$. The energy of the highest TS for each reaction pathway is marked blue. Asterisks (*) indicate elongated bonds.

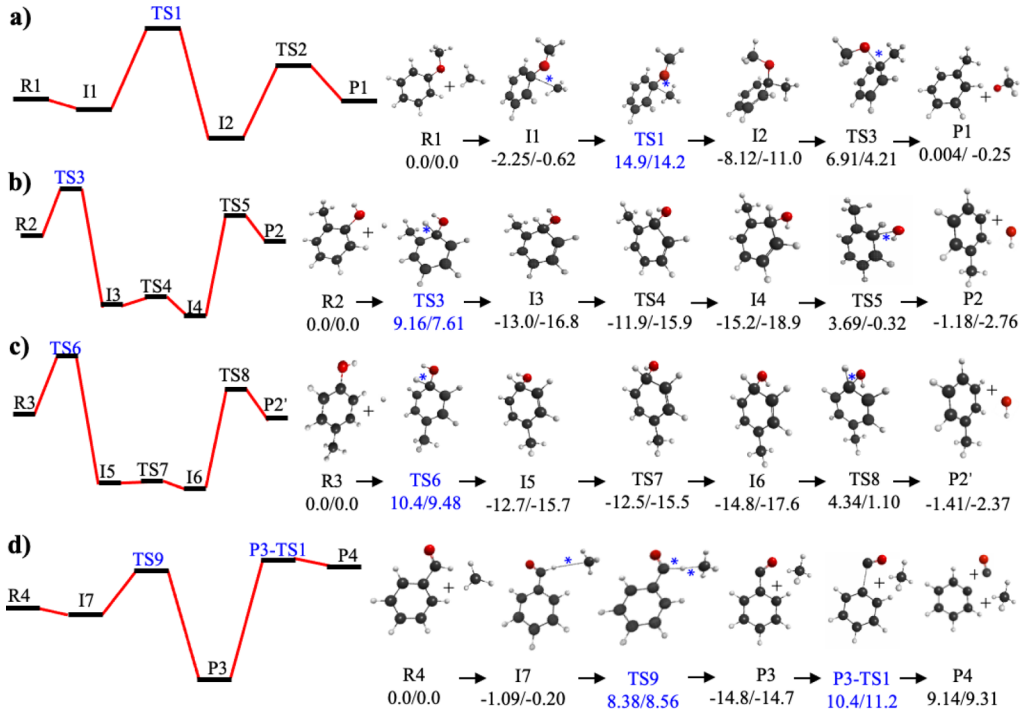

Figure 7. Reaction pathways for formation of toluene (a–c) and phenyl (d): (a) anisole + CH_3, (b) *o*-cresol + H, (c) *p*-cresol + H, and (d) benzaldehyde + H. The relative energies (kcal/mol) are reported in the format $E_{M06\text{-}2X}/E_{F12\text{-}CCSDT(T)}$. The energy of the highest TS for each reaction pathway is marked blue. Asterisks (*) indicate elongated bonds.

https://doi.org/10.1021/acs.energyfuels.1c00858
Energy Fuels 2021, 35, 9994–10008

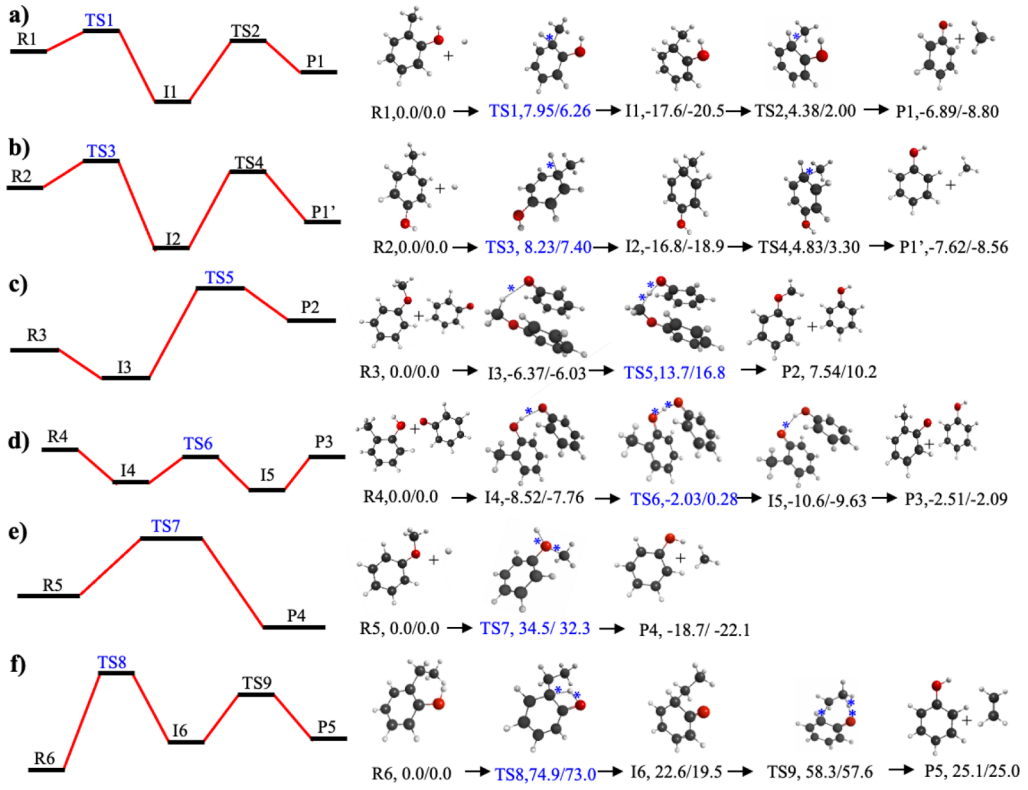

Figure 8. Reaction pathways for formation of phenol: (a) *o*-cresol + H, (b) *p*-cresol + H, (c) anisole + phenoxy, (d) *o*-cresol + phenoxy, (e) anisole + H, and (f) dissociation of *o*-ethylphenol. The relative energies (kcal/mol) are reported in the format $E_{\text{M06-2X}}/E_{\text{F12-CCSDT(T)}}$. The energy of the highest TS for each reaction pathway is marked blue. Asterisks (*) indicate elongated bonds.

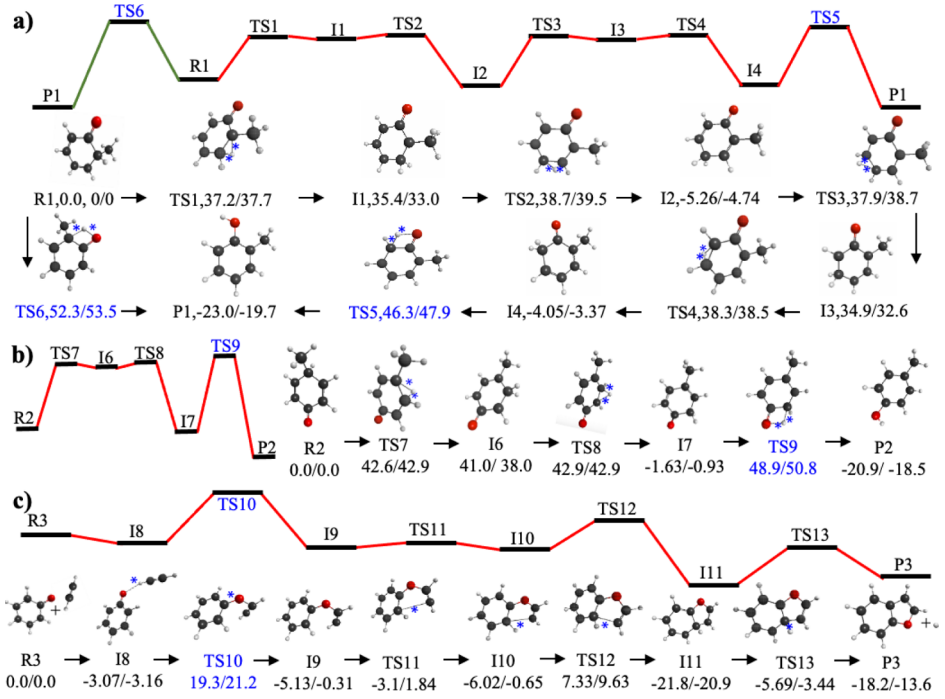

Figure 9. Reaction pathways for formation of cresol (a,b) and benzofuran (c): (a) rearrangement of *o*-methylcyclohexadienone (the red and green lines show different reaction paths), (b) rearrangement of *p*-methylcyclohexadienone, and (c) reaction of the phenoxy radical with acetylene. The relative energies (kcal/mol) are reported in the format $E_{\text{M06-2X}}/E_{\text{F12-CCSDT(T)}}$. The energy of the highest TS for each reaction pathway is marked blue. Asterisks (*) indicate elongated bonds.

methylcyclopentadiene and CO and isomerize to cresol, which is a precursor of toluene and many other oxygenated products. The CH_3 radical can undergo H-abstraction to form methane or recombine with another CH_3 to produce ethane. Cyclopentadienyl, another important intermediate, is responsible for the formation of 1,3-cyclopentadiene and methylcyclopenta-

https://doi.org/10.1021/acs.energyfuels.1c00858
Energy Fuels 2021, 35, 9994−10008

Table 1. Compounds Detected in the Experiments at Different Temperatures and the Corresponding Reactions with Predicted Energy Barriers (ΔE)

compound	temperature (°C) 400	450	500	550	600	650	reaction number	reaction	ΔE (kcal/mol)
benzene	+	+	+	+	+	+	R1	anisole + H → benzene + CH_3	8.17
							R2	anisole + CH_3 → anisyl + CH_4 → benzene + HCO + CH_4	21.2
							R3	benzaldehyde + H → benzene + HCO	7.42
							R4	phenol + H → benzene + OH	9.02
							R5	methylcyclopentadiene → methylenecyclopentadiene + H → cyclohexadienyl → benzene + 2H[b]	75−85[a]
							R6	5-methylcyclopentadiene → fulvene + H_2 → benzene + H_2	101.1
toluene	−	+	+	+	+	+	R7	anisole + CH_3 → toluene + CH_3O	14.8
							R8	*o*-cresol + H → toluene + OH (*p*-cresol + H → toluene + OH)	7.61 (9.48)
							R9	benzaldehyde + CH_3 → benzoyl + CH_4 → phenyl + CO + CH_4	25.9
								phenyl + CH_3 → toluene	102.0[a]
benzofuran	−	−	+	+	+	+	R10	phenoxy + C_2H_2 → benzofuran + H	24.4
							R11	*o*-ethylphenol → 4H + benzofuran[c]c	
1-methylcyclopentadiene/2-methylcyclopentadiene	−	−	+	+	+	+	R12	cyclopentadienyl + CH_3 → 5-methylcyclopentadiene	−69.9[a]
								5-methylcyclopentadiene → 1-methylcyclopentadiene	24.6
							R13	*p*-methylphenoxy → methylcyclopentadienyl + CO (*o*-methylphenoxy → methylcyclopentadienyl + CO)	53.5 (54.7)
								methylcyclopentadienyl + H → 1-methylcyclopentadiene/2-methylcyclopentadiene	73.9[a]/73.7[a]
							R14	*o*-methylcyclohexadienone → 1-methylcyclopentadiene + CO	57.3
							R15	*p*-methylcyclohexadienone → 1-methylcyclopentadiene + CO	60.1
							R16	*o*-methylcyclohexadienone → 2-methylcyclopentadiene + CO	64.2
							R17	*p*-methylcyclohexadienone → 2-methylcyclopentadiene + CO	75.8
benzaldehyde	−	−	−	+	+	−	R18	anisole + CH_3 → anisyl + CH_4 → benzaldehyde + H + CH_4	20.1
1,3-cyclopentadiene	−	−	−	+	+	+	R19	phenoxy → cyclopentadienyl + CO	53.2
								cyclopentadienyl + H	−81.2[a]
ethylbenzene	−	−	−	+	+	+	R20	cyclopentadienyl + C_2H_2 → benzyl	45.2
								benzyl + C_2H_2 → ethylbenzene	−76.6[a]
styrene	−	−	−	+	+	+	R21	cyclopentadienyl + C_3H_3 → 5-propadienylcyclopentadiene	60.5[a]
								5-propadienylcyclopentadiene → styrene	63.6
o-xylene	−	−	−	+	+	+	R22	toluene + CH_3 → *o*-methylphenyl + CH_4	16.9
								o-methylphenyl + CH_3 → *o*-xylene	−101.8[a]
phenol	−	−	−	−	+	−	R23	phenoxy + H → phenol	−85.7[a]
							R24	*o*-cresol + H → phenol + CH_3 (*p*-cresol + H → phenol + CH_3)	6.26 (7.40)
							R25	anisole + phenoxy → phenol + anisyl	22.8
							R26	*o*-cresol + phenoxy → phenol + methylphenoxy	8.04
							R27	anisole + H → phenol + CH_3	32.3
							R28	*o*-ethylphenol → phenol + C_2H_4	73.0
o-cresol	−	−	−	−	+	−	R29	*o*-methylcyclohexadienone → *o*-cresol	52.6
p-cresol	−	−	−	−	+	−	R30	*p*-methylcyclohexadienone → *p*-cresol	51.7
indene	−	−	−	−	+	+	R31	cyclopentadienyl + C_4H_6 → C_9H_9 + H_2 → indene + H_2 + H	45.3

[a]For barrierless reactions, the reported values are the energies of products with respect to reactants. [b]Reaction mechanism from ref 66. [c]Reaction mechanisms from ref 42.

https://doi.org/10.1021/acs.energyfuels.1c00858
Energy Fuels 2021, 35, 9994−10008

diene and many aromatic compounds, including benzene, styrene, ethylbenzene, indene, and naphthalene. At the same time, at low temperatures, anisole can decompose through bimolecular reactions with hydrogen, methyl, and phenoxy radicals, as summarized in Figure 5. The ipso-substitution and H-atom abstraction reactions can lead to the formation of several aromatic products. The reaction mechanisms for the products observed in the experiments and some products reported in the literature,[13,29,36,37,41,42,44,68] including cyclopentadiene, methylcyclopentadiene, benzene, toluene, aromatics, and oxygenated aromatics, are shown in Figures 6−9 and S5−S7 and discussed in detail below.

Table 1 lists the compounds that were detected in the experiments at the temperatures from 400 to 650 °C and the corresponding reactions with energy barriers leading to these compounds. At low temperatures of 400 and 450 °C, only benzene and toluene were detected, which can be explained by the low energy barriers of the bimolecular ipso-addition reactions of H and CH_3 radicals at the methoxy moiety of anisole (reactions R1 and R7). At higher temperatures, benzene is formed during the decomposition of methylcyclopentadiene (R5 and R6); the latter is formed mainly in the decomposition of methylcyclohexadienone (R14−R17). Cyclopentadiene is formed through the recombination of the H atom and the cyclopentadienyl radical produced from the high barrier decomposition of phenoxy (R19). As temperature increased, other aromatics including ethylbenzene (R20), styrene (R21), *o*-xylene (R22), and indene were observed. The energy barrier of the *o*-xylene formation is low because the CH_3 radical abstracts a benzylic H atom from toluene more easily than a phenylic H atom.[69] Once benzyl is formed, it can recombine with CH_3 to form ethylbenzene. At 500 °C, benzofuran, the first oxygenated compound, was detected. Phenol and benzaldehyde were not observed at this temperature, likely because they are quickly consumed in the reactions with other compounds. While phenol can be easily formed from the low-barrier H-abstraction on cresol or anisole (R24−R25) or from the barrierless recombination of the phenoxy and H atom (R23), the following reactions with H (R4) and C_2H_2 (R10) are expected to consume phenol quickly. The bimolecular reaction of anisole and CH_3 (R18) contributes to the formation of benzaldehyde with a relatively low energy barrier. However, the H atom ipso-addition (R3) and abstraction (R9) are likely to reduce the amount of benzaldehyde. At 600 °C, cresol was detected, which correlates with the relatively high reaction barrier of the methylcyclohexadienone to cresol rearrangement (R29 and R30). Similar to phenol, cresol can be consumed at high temperatures (it was not detected at 650 °C), serving as a precursor of toluene (R8) and phenol (R24 and R26). Therefore, there is a good agreement between the compounds detected in the experiments performed at different temperatures and the energy barriers obtained from the electronic structure calculations.

3.2.1. Formation of Benzene and Toluene. Benzene and toluene are the only two products detected at temperatures below 500 °C, with benzene detected at a temperature as low as 400 °C. Three calculated pathways of benzene formation are depicted in Figure 6. These include two bimolecular reactions (Figure 6a,b) and a unimolecular reaction (Figure 6c). The low-temperature formation of benzene is mostly originated from an ipso-addition of an H atom[1,41] at the methoxy moiety of anisole. As seen in Figure 6a, the initial reaction of anisole with an H radical must overcome the rate-determining TS1 with a barrier of 8.17 kcal/mol to produce encounter complex I1, which is characterized by the formation of an additional C−H bond. The intermediate I1 undergoes scission of the C−O bond (I1 → TS2 → P1), leading to the liberation of the OCH_3 radical and formation of benzene. The small barrier suggests that this is the most favorable reaction pathway at low temperatures, in good agreement with the small activation energy of 7.93 kcal/mol adopted by Nowakowska et al.[41] A similar ipso-addition of an H atom can also occur with benzaldehyde and phenol (Figure S5a,b), contributing to the observed decline in the concentration of these species at higher temperatures.

To produce benzene, anisole decomposition can also proceed through the bimolecular mechanism of H-abstraction by CH_3, H, or phenoxy radicals to produce an anisyl radical. The latter can isomerize to form a benzoxyl radical, which decomposes to benzene and HCO. Here, we only discuss details of the H-abstraction by a CH_3 radical (Figure 6b), which was first reported by Mulcahy et al.[24] First, CH_3 and anisole barrierlessly form unstable encounter complex I2. Then, CH_3 abstracts an H atom from the methoxy group (I2 → TS3 → P2) by overcoming a barrier of 15.6 kcal/mol to form the unstable anisyl radical and methane. As reported in theoretical studies on benzaldehyde[70] and benzoxyl[71] decomposition, the subsequent cyclization (P2 → P2-TS1 → P2-I1) can lead to the formation of an intermediate with a three-member ring, followed by a ring-opening reaction (P2-I1 → P2-TS2 → P2-I2), resulting in a benzoxyl radical P2-I2, which can serve as a branch point for formation of different species. On one hand, the reaction can proceed through the intramolecular hydrogen shift (P2-I2 → P2-TS3→ P2-I3) from CH_2O to a C atom on the aromatic ring, followed by breakage of the C−C bond (P2-I3 → P2-TS4 → P3) to form benzene and CHO. The intramolecular hydrogen shift is the rate-determining step with the barrier of 21.2 kcal/mol, which is higher than that of the reaction of anisole and H (Figure 6a). This indicates that the intramolecular hydrogen shift pathway to benzene formation is less energetically favorable than the reaction of anisole and H radical. On the other hand, as reported previously,[24,29] one of C−H bonds in the CH_2O moiety of the benzoxyl radical can break (P2-I2 → P2-TS5 → P4) by overcoming a slightly lower barrier of 20.1 kcal/mol to form H and benzaldehyde. This supports the fact that benzaldehyde was detected at the relatively low temperature of 550 °C and agrees well with the larger activation energy of benzene formation than that of benzaldehyde formation predicted by Nowakowska, et al.[41]

In addition, decomposition of three methylcyclopentadiene isomers is responsible for the formation of a large amount of benzene at high temperatures. The reaction mechanism is very complex as described in several studies,[66,67,72,73] with some important reaction pathways shown in Figure 4. First, methylcyclopentadiene isomers can undergo a one-step H-elimination to generate three isomers of the methylenecyclopentadiene radical.[66] This radical can undergo a ring expansion, leading to the cyclohexadienyl radical (C_6H_7), which can produce benzene by a fast H-atom ejection. Second, two consecutive H-atom eliminations from methylcyclopentadiene can take place, that is, one more H-atom elimination occurs after the formation of methylenecyclopentadiene, leading to fulvene.[73] In a recent study of anisole pyrolysis, fulvene was shown to play an important role in benzene formation.[13] Another pathway to fulvene through H_2 loss from

https://doi.org/10.1021/acs.energyfuels.1c00858
Energy Fuels 2021, 35, 9994−10008

5-methylcyclopentadiene is depicted in Figure 6c. The relatively low isomerization barrier of 24.6 kcal/mol indicates that 5-methylcyclopentadiene can easily isomerize to 1-methylcyclopentadiene, which also explains why 5-methylcyclopentadiene is not detected in the experiments. In contrast to the direct 1,1-H_2 and 1,2-H_2 eliminations from 5-methylcyclopentadiene,[60] in this mechanism, an H_2 molecule is formed by one H atom from the CH_3 moiety and another H atom from the five-member ring, leading to the formation of fulvene with the barrier of 100.7 kcal/mol. Fulvene can undergo a similar ring expansion through a bicyclic intermediate (P5 → P5-TS1 → P5-I1 → P5-TS2 → P5-I2) to produce a six-member ring compound P5-I2, which leads to benzene after an H-shift on the six-member ring (P5-I2 → P5-TS3 → P6). The H atom can also assist the conversion from fulvene to benzene with a significantly lower energy barrier of 52.3 kcal/mol predicted by the BAC-MP4 level of theory.[67] However, it is obvious that the overall barriers for the methylcyclopentadiene-to-benzene pathways are very high (at least 70 kcal/mol), which explains the fact[1,41] that methylcyclopentadiene only contributes to benzene formation at high temperatures.

Toluene was the second aromatic product detected at 450 °C. The four studied pathways of toluene formation are shown in Figure 7. Similar to the reaction of anisole with an H radical, anisole can react with a CH_3 radical through the ipso-addition of CH_3 at the methoxy moiety (Figure 7a). The encounter complex I1 stabilized by only 0.62 kcal/mol with respect to the reactants is formed in the barrierless reaction, followed by the CH_3 binding to the carbon ring. The barrier of this bimolecular reaction is 14.8 kcal/mol, higher than that of benzene formation in Figure 6a. This agrees well with the larger activation energy for toluene formation compared to that of benzene,[41] which may explain why toluene was detected at a higher temperature than benzene in our experiments.

Toluene can also be formed from decomposition of oxygenated compounds, such as *o*/*p*-cresol[44] and benzaldehyde. The reaction mechanism for conversion of the two isomers of cresol to toluene is shown in Figure 7b,c. These reactions proceed through an H atom ipso-addition at the hydroxyl site in cresol. In contrast to the reaction of anisole and H, the C−O bond rotation (I3 → TS4 → I4 for *o*-cresol and I5 → TS7 → I6 for *p*-cresol) is allowed after the initial formation of an additional C−H bond. This is the rate-determining step with the barriers of 7.61 and 9.48 kcal/mol for *o*- and *p*-cresol, respectively. The relatively low barriers agree well with a previous study, showing that ipso-addition reaction between cresol and H plays a significant role in the consumption of cresol.[44]

Figure 7d shows another major reaction leading to the formation of toluene. As shown in a previous report,[37] a CH_3 radical can abstract an H atom from the CHO group in benzaldehyde (I7 → TS9 → P3) to produce benzoyl and methane. Benzoyl can eliminate CO directly by breaking the C−O bond (P3 → P3-TS1 → P4) to form a phenyl radical. In turn, the phenyl can generate toluene by recombining with the CH_3 radical and releasing 102.0 kcal/mol energy (Figure 5). The overall barrier of this reaction is only 25.9 kcal/mol, which supports the decline of benzaldehyde concentration at high temperatures in the experiments.

3.2.2. Formation of Oxygenated Aromatics. Several oxygenated aromatic compounds produced during the decomposition of anisole were detected in the experiments (Figure 3). In addition to the benzaldehyde formation mechanism discussed above, reaction mechanisms leading to the formation of phenol, cresol, and benzofuran were investigated using electronic structure methods (Figures 8 and 9).

Six reaction pathways leading to the formation of phenol are displayed in Figure 8. The ipso-addition reaction of H to cresol can be initiated on the OH moiety to produce toluene (Figure 7b) or on the CH_3 moiety, leading to phenol[44] (Figure 8a,b). The highest energy barriers for these reactions are only 6−8 kcal/mol, which suggests that cresol is an important precursor to both toluene and phenol. Another common source of phenol is the H-abstraction by the phenoxy radical from hydrogen donors, such as anisole (Figure 8c) and cresol (Figure 8d), leading to additional products—anisyl and methylphenoxy radicals, respectively. The barrier for the H-abstraction from the CH_3 group in anisole (22.8 kcal/mol) is much higher than that from the OH group in cresol (8.04 kcal/mol), which agrees well with the reported activation energies of 16.06 kcal/mol and 9.50 kcal/mol for anisole and cresol, respectively.[36] Note that a phenoxy radical can also abstract an H atom form the CH_3 group in cresol (Figure S5c), yielding *o*-hydroxybenzyl, but this requires overcoming a higher barrier of 17.8 kcal/mol. Apart from H-abstraction, phenoxy and H radicals can recombine with an experimentally determined rate constant of 2.5×10^{14} s^{-1},[74] leading to the direct formation of phenol and energy release of 85.7 kcal/mol (Figure 4). Besides, the ipso-addition of an H radical to the CH_3 moiety in anisole[13,30] can also generate phenol, as shown in Figure 8d. In contrast to the ipso-addition, a concerted reaction takes place through single TS7, leading to the formation of an O−H bond and concomitant breakage of the C−O bond. However, the energy barrier of 32.3 kcal/mol is high, indicating a negligible contribution of this reaction to phenol formation, at least at low temperatures. In addition, phenol can be obtained from the dissociation of *o*-ethylphenol produced in the reaction of methyl and hydroxybenzyl radicals.[41] Figure 8f shows a two-step H-transfer mechanism of *o*-ethylphenol dissociation, which is different from the previously described one-step H-transfer through a four-member ring TS.[42] This reaction involves an intramolecular H-shift from the OH group to the aromatic ring through the rate-determining TS8 (73.0 kcal/mol), leading to the intermediate I6. Then, the reaction proceeds through the six-member ring TS9 characterized by a second H-shift from the CH_3 group to the O atom with a concomitant breakage of the C−C bond, generating phenol and ethylene. Because of the lower barrier, this two-step reaction is expected to be more favorable than the previously reported one-step reaction[42] and is responsible for consuming *o*-ethylphenol at high temperatures.

Cresol can be formed via a methylcyclohexadienone intermediate[36] produced by methyl addition to the phenoxy radical at the *ortho* or *para* position.[75] The mechanism of isomerization from *o*/*p*-methylcyclohexadienone to *o*/*p*-cresol is shown in Figure 9a,b. For *o*-methylcyclohexadienone, the four-step H-migration between adjacent carbon atoms of the aromatic ring (R1 → TS1 → I1 → TS2 → I2 → TS3 → I3 → TS4 → I4) helps in triggering the final H-shift from the carbon to oxygen atom (I4 → TS5 → P1) and produce *o*-cresol by overcoming the barrier of 52.6 kcal/mol with respect to the intermediate I2. The resonance-stabilized intermediates I2 and I4 are the other two stable isomers of *o*-methylcyclohex-

https://doi.org/10.1021/acs.energyfuels.1c00858
Energy Fuels 2021, 35, 9994−10008

adienone. Alternately, *o*-methylcyclohexadienone can undergo an H-shift (R1 → TS6 → P1) directly from the carbon to oxygen atom, forming *o*-cresol by overcoming a little higher barrier of 53.5 kcal/mol. Thus, based on energetics, the former mechanism of the multi-step H-shift is expected to dominate in the formation of cresol. For *p*-methylcyclohexadienone, isomerization to *p*-cresol can take place through a two-step H-migration between neighboring carbon atoms (R2 → TS7 → I6 → TS8 → I7) and the final H-shift from carbon to oxygen (I7 → TS9 → P2) with a barrier of 51.7 kcal/mol. This reaction, proceeding through a stable isomer of *p*-methylcyclohexadienone I7, is the only pathway leading to *p*-cresol. The calculated lower barrier for multi-step H-shift leading to *o*-cresol and the predicted single pathway to *p*-cresol agree well with the results reported for the reaction between phenoxy and CH_3 radicals.[42]

Benzofuran is another oxygenated product detected in the experiment. As recently reported,[13,42] *o*-ethylphenol, formed by recombination of hydroxylbenzyl and methyl radicals, is a major source of benzofuran. *o*-Ethylphenol can undergo a two-step H-elimination reaction to reach *o*-ethenylphenol, which can further lose a hydrogen atom to produce an *o*-ethenylphenoxy radical. The intermolecular cyclization and subsequent H-elimination lead to the formation of benzofuran. This pathway with the known rate constant parameters[42] also contributes to the consumption of *o*-ethylphenol at high temperatures. Similarly, a stepwise dehydrogenation of *o*-methylanisole with subsequent cyclization and H-elimination can lead to benzofuran, as seen in Figure 4. In addition, benzofuran was found to be produced from the decomposition of phenoxyacetylene,[76] which is formed by recombination of the phenoxy radical and acetylene (Figure 9c). Acetylene and the phenoxy radical form a weakly bound intermediate I8 without a barrier. Then, the addition reaction I8 → TS10 → I9 must overcome a barrier of 24.4 kcal/mol to generate phenoxyacetylene (I9). The subsequent bond rotation I9 → TS11 → I10 helps the CH group to face the nearby carbon atom of the aromatic ring and induces the intramolecular cyclization I10 → TS12 → I11 to form a closed-ring intermediate I11. Finally, the hydrogen elimination I11 → TS13 → P3 generates benzofuran. It was found that I9 can also directly undergo the ring-closing reaction to I11[76] with a similar barrier. As the overall barrier is not very high, the pathway in Figure 9c is expected to contribute to benzofuran formation, if acetylene is present in significant quantities.

3.2.3. Formation of Cyclopentadiene, Methylcyclopentadiene, and Additional Aromatic Hydrocarbons. Apart from benzene and toluene, other hydrocarbon products of anisole decomposition are cyclopentadiene, methylcyclopentadiene, and aromatic hydrocarbons including styrene, ethylbenzene, *o*/*p*-xylene, and indene. The reaction mechanisms of their formation are shown in Figures S6 and S7. The previously studied high-temperature recombination of two cyclopentadienyl radicals and decomposition of the cyclopentadienyl radical[37,65] to form naphthalene and C_3H_3 radical + C_2H_2, respectively, will not be discussed here because this work focuses on anisole decomposition at temperatures not higher that 650 °C.

As mentioned above, the cyclopentadienyl radical serves as a precursor to styrene, ethylbenzene, indene, methylcyclopentadiene, naphthalene, and small hydrocarbons. It is well known that the phenoxy radical decomposition is responsible for the formation of the cyclopentadienyl radical. As seen in Figure S6a, the phenoxy radical can undergo an intermolecular cyclization R1 → TS1 → I1 to form a bicyclic intermediate I1, followed by a ring-opening reaction I1 → TS2 → I2 to produce a 2,4-cyclpentadienyl carbonyl radical I2. The subsequent scission of the C−C bond (I2 → TS3 → P1) leads to a cyclopentadienyl radical and CO. The second rate-determining step has a barrier of 53.2 kcal/mol, which is consistent with previous studies.[17,33−35] Once the cyclopentadienyl radical is formed, 1,3-cyclopentadiene can be generated through recombination with H or H-abstraction from a hydrogen donor.

Formation of styrene can proceed through isomerization of 5-propadienylcyclopentadiene that derived from the recombination of cyclopentadienyl and C_3H_3 radicals.[77] As seen in Figure S6b, a hydrogen atom can shift from the carbon atom bonded to the five-member ring to the middle carbon of the propadienyl group (R2 → TS4 → I3), leading to the formation of a three-ring intermediate I3. To reach styrene, two C−C bonds must be broken in a ring-opening reaction I3 → TS5 → P2. The overall energy barrier of 63.6 kcal/mol indicates that the formation of styrene is unlikely to occur at low temperatures.

In a study of toluene oxidation, it was reported that cyclopentadienyl can also recombine with C_2H_2 to form a benzyl radical,[78] which can further recombine with CH_3 to produce ethylbenzene, releasing 76.6 kcal/mol energy, as seen in Figure 4. A reaction pathway for benzyl formation is depicted in Figure S6c. The initial barrier-free reaction of cyclopentadienyl and C_2H_2 gives rise to a complex I4. Then, the reaction proceeds through an addition I4 → TS6 → I5 and an H-shift I5 → TS7 → I6, overcoming a barrier of 45.2 kcal/mol. Starting from I6, similar to the decomposition of the methylenecyclopentadiene radical leading to benzene, the ring expansion I6 → TS8 → I7 → TS9 → P3 occurs through a bicyclic intermediate, leading to a benzyl radical. The relative energies calculated for this reaction pathway agree well with those of the reverse decomposition of benzyl radicals.[79]

o/*p*-Xylene can be formed by recombination of CH_3 with an *o*/*p*-methylphenyl radical generated by H-abstraction from the toluene ring[69] Taking the *o*-methylphenyl radical as an example, the reaction pathway of H-abstraction is shown in Figure S6d. The barrier of 16.9 kcal/mol is in good agreement with the activation energy of 15.0 kcal/mol predicted by Bounaceur et al.[69] Indene is another aromatic product of anisole decomposition. The reaction pathway for its formation from cyclopentadienyl and 1,3-butadiene (C_4H_6) reported in a recent study[13] is depicted in Figure S6e. The direct addition reaction leads to a stable intermediate I8 with one new C−C bond formed. To form indene, several reaction steps must occur, including a H-shift on the five-member ring I8 → TS11 → I9, a six-member ring closure (I9 → TS12 → I10), an H-shift on the six-member ring (I10 → TS13 → I11), elongation of the C−H bond (I11 → TS14 → I12), and H−H bond formation (I12 → TS15 → I12), leading to a C_9H_9 radical and H_2. Finally, the C_9H_9 radical can lose a hydrogen atom (P5 → P5-TS1 → P6) to form indene. The high overall barrier of 45.3 kcal/mol explains why in our experiments, indene was detected only at a relatively high temperature of 600 °C.

Methylcyclopentadiene, apart from the abovementioned reaction of the cyclopentadienyl radical (C_5H_5) and CH_3, can be produced by dissociation of an *o*/*p*-methylphenoxy radical[36] and *o*/*p*-methylcyclohexadinenone.[42] *o*/*p*-Methylphenoxy radicals can be formed through H-abstraction from the

https://doi.org/10.1021/acs.energyfuels.1c00858
Energy Fuels 2021, 35, 9994−10008

OH group of cresol or H fission in *o*/*p*-methylcyclohexadienone, which also serves as a major source of H atoms.[42] The reaction pathways for the dissociation of an *o*/*p*-methylphenoxy radical are shown in Figure S7a,b. These pathways include the initial cyclization, ring opening, and final scission of the C−C bond, yielding CO and a methylcyclopentadienyl radical. The latter recombines with an H atom to form methylcyclopentadiene. The overall mechanism and energy barriers are similar to those of phenoxy radical decomposition, indicating that the presence of the CH_3 group has almost no effect on the phenoxy decomposition reported by Carstensen and Dean.[35] In addition, *o*/*p*-methylcyclohexadienone can not only rearrange to *o*/*p*-cresol (Figure 9a,b) but also dissociate to methylcyclopentadiene and CO, as seen in Figure S7c,d. During the decomposition of *o*-methylcyclohexadienone (Figure S7c), several H-migration steps lead to the formation of two unstable isomers I5 and I7. These isomers can proceed through cyclization and C−C bond scission (I5 → TS11 → I9 → TS12 → P2, I7 → TS13 → I10 → TS14 → P3) to generate 1-methylcyclopentadiene and 2-methylcyclopentadiene, with a barrier of 57.3 kcal/mol (TS12 with respect to R3) for the former and 64.2 kcal/mol (TS14 with respect to I6) for the latter. Other higher barrier pathways involving the stable isomer I8 of *o*-methylcyclohexadienone were also found. The initial ring opening (R3 → TS15 → I11, I8 → TS18 → I13) is followed by cyclization and C−C bond scission (I11 → TS16 → I12 → TS17 → P4, I13 → TS19 → I9 → TS12 → P2) to form 5-methylcyclopentadiene and 1-methylcyclopentadiene, respectively, with a barrier of 74.7 kcal/mol (TS16 with respect to R3) for the former and 78.5 kcal/mol (TS19 with respect to I6) for the latter. The decomposition of *p*-methylcyclohexadienone (Figure S7d) proceeds similarly to that of *o*-methylcyclohexadienone; however, the reaction mechanism is much simpler. After several steps, the isomeric intermediates I15 and I14 produce 2-methylcyclopentadiene and 1-methylcyclopentadiene by overcoming the barriers of 75.8 kcal/mol (TS23 with respect to I15) and 60.1 kcal/mol (TS26 with respect to R4), respectively. In agreement with the energy barriers reported by Koirala,[42] the predicted barriers for the formation of 2-methylcyclopentadiene from the dissociation of *o*/*p*-methylcyclohexadienone are the lowest, and the barrier for the formation of 5-methylcyclopentadiene is the highest. Also, 5-methylcyclopentadiene is predicted to be the most thermodynamically unstable isomer. This indicates that formation of 5-methylcyclopentadiene is not favorable and supports the fact that it was not detected in our experiments.

4. CONCLUSIONS

To better understand the mechanism of low-temperature anisole pyrolysis, we studied the decomposition of anisole in the gas phase at temperatures from 300 to 650 °C. The decomposition products were analyzed with the GC−MS/FID technique. Benzene was the lowest-temperature product detected at 400 °C. This is the lowest temperature for anisole decomposition that has been reported to date. Toluene, the second low-temperature product, was detected at 450 °C. Many other decomposition products were observed at temperatures above 450 °C, including aromatics, oxygenated aromatics, nonaromatic C1−C6 hydrocarbons, and different light compounds. Detailed mechanistic studies with the DFT and high-level coupled cluster methods revealed multiple unimolecular and biomolecular reaction pathways leading to the formation of primary products of anisole decomposition. The predicted energies of TSs and intermediates helped us to identify the dominant reaction pathways at different temperatures. Formation of benzene and toluene at low temperatures (400−450 °C) is explained by the low-energy barrier ipso-addition of CH_3 and H radicals at the methoxy moiety of anisole. At 500−550 °C, multiple complex reaction mechanisms lead to the formation of benzofuran, methylcyclopentadiene, benzaldehyde, cyclopentadiene, ethylbenzene, styrene, and *o*-xylene. Finally, at 600−650 °C, indene is formed through the reaction mechanisms with a relatively high energy barrier. Phenol and cresol are detected only at 600 °C, likely because at the other temperatures, they are quickly consumed in the reactions with other compounds. The good agreement between the compounds detected in the experiments performed at different temperatures and the energy barriers obtained from the electronic structure calculations demonstrates the power of the combined experimental and computational approach for elucidating the dominant mechanisms of complex molecular decompositions. The obtained results are expected to contribute to the development of predictive kinetic models for the decomposition of anisole and other oxygen-containing benzene derivatives playing an important role in the biomass pyrolysis for production of valuable chemicals and fuels.

■ ASSOCIATED CONTENT

Supporting Information

The Supporting Information is available free of charge at https://pubs.acs.org/doi/10.1021/acs.energyfuels.1c00858.

Calibration of reactor temperature, GC−MS chromatograms of anisole decomposition, concentrations of C2−C5 volatile organic compounds detected by FID as functions of temperature, calculated reaction pathways for formation of benzene, phenol, cyclopentadiene, methylcyclopentadiene, and additional aromatic hydrocarbons, appearance of different compounds in GC−MS spectra at different temperatures, and atomic Cartesian coordinates of reactants, TSs, intermediates, and products (PDF)

■ AUTHOR INFORMATION

Corresponding Authors

Andrey Khlystov − *Organic Analytical Laboratory, Division of Atmospheric Sciences, Desert Research Institute, Reno, Nevada 89512, United States*; Email: andrey.khlystov@dri.edu

Sergey A. Varganov − *Department of Chemistry, University of Nevada, Reno, Nevada 89557-0216, United States*; orcid.org/0000-0001-8301-3891; Email: svarganov@unr.edu

Authors

Ting Zhang − *Department of Chemistry, University of Nevada, Reno, Nevada 89557-0216, United States; Organic Analytical Laboratory, Division of Atmospheric Sciences, Desert Research Institute, Reno, Nevada 89512, United States*

Chiranjivi Bhattarai − *Organic Analytical Laboratory, Division of Atmospheric Sciences, Desert Research Institute, Reno, Nevada 89512, United States*

Yeongkwon Son − *Organic Analytical Laboratory, Division of Atmospheric Sciences, Desert Research Institute, Reno,*

Nevada 89512, United States; orcid.org/0000-0002-4773-6838

Vera Samburova − *Organic Analytical Laboratory, Division of Atmospheric Sciences, Desert Research Institute, Reno, Nevada 89512, United States*

Complete contact information is available at: https://pubs.acs.org/10.1021/acs.energyfuels.1c00858

Author Contributions

T.Z., C.B., Y.S., V.S., and A.K. conducted the experiments. T.Z. and S.A.V. performed the electronic structure calculations. All authors contributed to the preparation of the manuscript. All authors have given approval to the final version of the manuscript.

Notes

The authors declare no competing financial interest.

■ ACKNOWLEDGMENTS

T.Z. was supported by the University of Nevada, Reno and Desert Research Institute Joint Postdoctoral Award. This work was partially supported by the National Science Foundation (NSF) through a CAREER Award (CHE-1654547) to S.A.V.

■ REFERENCES

(1) Wagnon, S. W.; Thion, S.; Nilsson, E. J. K.; Mehl, M.; Serinyel, Z.; Zhang, K.; Dagaut, P.; Konnov, A. A.; Dayma, G.; Pitz, W. J. Experimental and modeling studies of a biofuel surrogate compound: laminar burning velocities and jet-stirred reactor measurements of anisole. *Combust. Flame* **2018**, *189*, 325−336.

(2) Brown, R. *Thermochemical Processing of Biomass: Conversion into Fuels, Chemicals and Power*, 2nd ed.; John Wiley and Sons, 2019; pp 1−16.

(3) Wang, H.; Male, J.; Wang, Y. Recent advances in hydrotreating of pyrolysis bio-oil and its oxygen-containing model compounds. *ACS Catal.* **2013**, *3*, 1047−1070.

(4) Di Blasi, C. Modeling chemical and physical processes of wood and biomass pyrolysis. *Prog. Energy Combust. Sci.* **2008**, *34*, 47−90.

(5) Klose, W.; Wolki, M. On the intrinsic reaction rate of biomass char gasification with carbon dioxide and steam. *Fuel* **2005**, *84*, 885−892.

(6) Pan, H. Synthesis of polymers from organic solvent liquefied biomass: A review. *Renewable Sustainable Energy Rev.* **2011**, *15*, 3454−3463.

(7) McKendry, P. Energy production from biomass (part 1): overview of biomass. *Bioresour. Technol.* **2002**, *83*, 37−46.

(8) McCormick, R. L.; Ratcliff, M. A.; Christensen, E.; Fouts, L.; Luecke, J.; Chupka, G. M.; Yanowitz, J.; Tian, M.; Boot, M. Properties of oxygenates found in upgraded biomass pyrolysis oil as components of spark and compression ignition engine fuels. *Energy Fuels* **2015**, *29*, 2453−2461.

(9) Zhou, L.; Boot, M. D.; Johansson, B. H.; Reijnders, J. J. E. Performance of lignin derived aromatic oxygenates in a heavy-duty diesel engine. *Fuel* **2014**, *115*, 469−478.

(10) Boot, M. *Biofuels from Lignocellulosic Biomass: Innovations beyond Bioethanol*; John Wiley and Sons, 2016; pp 159−188.

(11) Britt, P. F.; Buchanan, A. C.; Cooney, M. J.; Martineau, D. R. Flash vacuum pyrolysis of methoxy-substituted lignin model compounds. *J. Org. Chem.* **2000**, *65*, 1376−1389.

(12) Custodis, V. B. F.; Hemberger, P.; Ma, Z.; van Bokhoven, J. A. Mechanism of fast pyrolysis of lignin: studying model compounds. *J. Phys. Chem. B* **2014**, *118*, 8524−8531.

(13) Yuan, W.; Li, T.; Li, Y.; Zeng, M.; Zhang, Y.; Zou, J.; Cao, C.; Li, W.; Yang, J.; Qi, F. Experimental and kinetic modeling investigation on anisole pyrolysis: Implications on phenoxy and cyclopentadienyl chemistry. *Combust. Flame* **2019**, *201*, 187−199.

(14) Faust, S.; Dreier, T.; Schulz, C. Photo-physical properties of anisole: temperature, pressure, and bath gas composition dependence of fluorescence spectra and lifetimes. *Appl. Phys. B* **2013**, *112*, 203−213.

(15) Tran, K. H.; Morin, C.; Kühni, M.; Guibert, P. Fluorescence spectroscopy of anisole at elevated temperatures and pressures. *Appl. Phys. B* **2013**, *115*, 461−470.

(16) Faust, S.; Goschütz, M.; Kaiser, S. A.; Dreier, T.; Schulz, C. A comparison of selected organic tracers for quantitative scalar imaging in the gas phase via laser-induced fluorescence. *Appl. Phys. B* **2014**, *117*, 183−194.

(17) Shu, B.; Herzler, J.; Peukert, S.; Fikri, M.; Schulz, C. A shock tube and modeling study about anisole pyrolysis using time-resolved CO absorption measurements. *Int. J. Chem. Kinet.* **2017**, *49*, 656−667.

(18) Talegaonkar, S.; Pandey, S.; Rai, N.; Rawat, P.; Sharma, H.; Kumari, N. Exploring nanoencapsulation of aroma and flavors as new frontier in food technology. *Encapsulations*; Academic Press, 2016; pp 47−88.

(19) Sharp, M. D.; Kocaoglu-Vurma, N. A.; Langford, V.; Rodriguez-Saona, L. E.; Harper, W. J. Rapid discrimination and characterization of vanilla bean extracts by attenuated total reflection infrared spectroscopy and selected ion flow tube mass spectrometry. *J. Food Sci.* **2012**, *77*, C284−C292.

(20) EFSA Panel on Food Contact Materials, Enzymes, Flavourings and Processing Aids (CEF). Scientific opinion on flavouring group evaluation 23, Revision 3 (FGE.23Rev3): aliphatic, alicyclic and aromatic ethers including anisole derivatives from chemical groups 15, 16, 22, 26 and 30. *EFSA J.* **2011**, *9*, 2398.

(21) Baker, R. R.; Bishop, L. J. The pyrolysis of tobacco ingredients. *J. Anal. Appl. Pyrolysis* **2004**, *71*, 223−311.

(22) Bansal, V.; Hashemi, B.; Raza, N.; Kim, K.-H.; Raza, W.; Kumar, P.; Brown, R. J. Review of the analytical methods for and clinical impact of additives and flavors used in electronic cigarettes. *Exposure Health* **2019**, *12*, 593.

(23) Rustemeier, K.; Stabbert, R.; Haussmann, H.-J.; Roemer, E.; Carmines, E. L. Evaluation of the potential effects of ingredients added to cigarettes. Part 2: Chemical composition of mainstream smoke. *Food Chem. Toxicol.* **2002**, *40*, 93−104.

(24) Mulcahy, M.; Tucker, B.; Williams, D.; Wilmshurst, J. Reactions of free radicals with aromatic compounds in the gaseous phase. III. Kinetics of the reaction of methyl radicals with anisole (methoxybenzene). *Aust. J. Chem.* **1967**, *20*, 1155−1171.

(25) Paul, S.; Back, M. H. A Kinetic determination of the dissociation energy of the C−O bond in anisole. *Can. J. Chem.* **1975**, *53*, 3330−3338.

(26) Schlosberg, R. H.; Szajowski, P. F.; Dupre, G. D.; Danik, J. A.; Kurs, A.; Ashe, T. R.; Olmstead, W. I. Pyrolysis studies of organic oxygenates. *Fuel* **1983**, *62*, 690−694.

(27) Lin, C.-Y.; Lin, M. C. Unimolecular decomposition of the phenoxy radical in shock waves. *Int. J. Chem. Kinet.* **1985**, *17*, 1025−1028.

(28) Suryan, M. M.; Kafafi, S. A.; Stein, S. E. The thermal decomposition of hydroxy- and methoxy-substituted anisoles. *J. Am. Chem. Soc.* **1989**, *111*, 1423−1429.

(29) Mackie, J. C.; Doolan, K. R.; Nelson, P. F. Kinetics of the thermal decomposition of methoxybenzene (anisole). *J. Phys. Chem.* **1989**, *93*, 664−670.

(30) Arends, I. W. C. E.; Louw, R.; Mulder, P. Kinetic study of the thermolysis of anisole in a hydrogen atmosphere. *J. Phys. Chem.* **1993**, *97*, 7914−7925.

(31) Colussi, A. J.; Zabel, F.; Benson, S. W. The very low-pressure pyrolysis of phenyl ethyl ether, phenyl allyl ether, and benzyl methyl ether and the enthalpy of formation of the phenoxy radical. *Int. J. Chem. Kinet.* **1977**, *9*, 161−178.

(32) Frank, P.; Herzler, J.; Just, T.; Wahl, C. High-temperature reactions of phenyl oxidation. *Symp. (Int.) Combust.* **1994**, *25*, 833−840.

(33) Olivella, S.; Sole, A.; Garcia-Raso, A. Ab Initio calculations of the potential surface for the thermal decomposition of the phenoxyl radical. *J. Phys. Chem.* **1995**, *99*, 10549−10556.
(34) Liu, R.; Morokuma, K.; Mebel, A. M.; Lin, M. C. Ab Initio study of the mechanism for the thermal decomposition of the phenoxy radical. *J. Phys. Chem.* **1996**, *100*, 9314−9322.
(35) Carstensen, H.-H.; Dean, A. M. A quantitative kinetic analysis of CO elimination from phenoxy radicals. *Int. J. Chem. Kinet.* **2012**, *44*, 75−89.
(36) Pecullan, M.; Brezinsky, K.; Glassman, I. Pyrolysis and oxidation of anisole near 1000 K. *J. Phys. Chem. A* **1997**, *101*, 3305−3316.
(37) Friderichsen, A. V.; Shin, E.-J.; Evans, R. J.; Nimlos, M. R.; Dayton, D. C.; Ellison, G. B. The pyrolysis of anisole ($C_6H_5OCH_3$) using a hyperthermal nozzle. *Fuel* **2001**, *80*, 1747−1755.
(38) Platonov, V. V.; Proskuryakov, V. A.; Ryl'tsova, S. V.; Popova, Y. N. Homogeneous pyrolysis of anisole. *Russ. J. Appl. Chem.* **2001**, *74*, 1047−1052.
(39) Wang, B.; Hou, H.; Yoder, L. M.; Muckerman, J. T.; Fockenberg, C. Experimental and theoretical investigations on the methyl−methyl recombination reaction. *J. Phys. Chem. A* **2003**, *107*, 11414−11426.
(40) Scheer, A. M.; Mukarakate, C.; Robichaud, D. J.; Ellison, G. B.; Nimlos, M. R. Radical chemistry in the thermal decomposition of anisole and deuterated anisoles: An investigation of aromatic growth. *J. Phys. Chem. A* **2010**, *114*, 9043−9056.
(41) Nowakowska, M.; Herbinet, O.; Dufour, A.; Glaude, P.-A. Detailed kinetic study of anisole pyrolysis and oxidation to understand tar formation during biomass combustion and gasification. *Combust. Flame* **2014**, *161*, 1474−1488.
(42) Koirala, Y. Investing the kinetics of anisole: a smiple lignin model compound. Ph.D. Thesis, Colorado School of Mines: Golen, CO, 2015.
(43) Wang, Q.-D.; Sun, M.-M.; Liang, J. Theoretical study of the hydrogen abstraction reactions from substituted phenolic species. *Comput. Theor. Chem.* **2021**, *1196*, 113120.
(44) Hemings, E. B.; Bozzano, G.; Dente, M.; Ranzi, E. Detailed kinetics of the pyrolysis and oxidation of anisole. *Chem. Eng. Trans.* **2011**, *24*, 61−66.
(45) Debiagi, P. E. A.; Gentile, G.; Pelucchi, M.; Frassoldati, A.; Cuoci, A.; Faravelli, T.; Ranzi, E. Detailed kinetic mechanism of gas-phase reactions of volatiles released from biomass pyrolysis. *Biomass Bioenergy* **2016**, *93*, 60−71.
(46) Büttgen, R. D.; Tian, M.; Fenard, Y.; Minwegen, H.; Boot, M. D.; Heufer, K. A. An experimental, theoretical and kinetic modelling study on the reactivity of a lignin model compound anisole under engine-relevant conditions. *Fuel* **2020**, *269*, 117190.
(47) Pelucchi, M.; Faravelli, T.; Frassoldati, A.; Ranzi, E.; Sri Bala, G.; Marin, G. B.; Van Geem, K. M. Experimental and kinetic modeling study of pyrolysis and combustion of anisole. *Chem. Eng. Trans.* **2018**, *65*, 127−132.
(48) Wu, Y.; Rossow, B.; Modica, V.; Yu, X.; Wu, L.; Grisch, F. Laminar flame speed of lignocellulosic biomass-derived oxygenates and blends of gasoline/oxygenates. *Fuel* **2017**, *202*, 572−582.
(49) Bierkandt, T.; Hemberger, P.; Oßwald, P.; Krüger, D.; Köhler, M.; Kasper, T. Flame structure of laminar premixed anisole flames investigated by photoionization mass spectrometry and photoelectron spectroscopy. *Proc. Combust. Inst.* **2019**, *37*, 1579−1587.
(50) Pelucchi, M.; Cavallotti, C.; Cuoci, A.; Faravelli, T.; Frassoldati, A.; Ranzi, E. Detailed kinetics of substituted phenolic species in pyrolysis bio-oils. *React. Chem. Eng.* **2019**, *4*, 490−506.
(51) Dente, M.; Ranzi, E.; Goossens, A. G. Detailed prediction of olefin yields from hydrocarbon pyrolysis through a fundamental simulation model (SPYRO). *Comput. Chem. Eng.* **1979**, *3*, 61−75.
(52) Ledesma, E. B.; Campos, C.; Cranmer, D. J.; Foytik, B. L.; Ton, M. N.; Dixon, E. A.; Chirino, C.; Batamo, S.; Roy, P. Vapor-phase cracking of eugenol: distribution of tar products as functions of temperature and residence time. *Energy Fuels* **2013**, *27*, 868−878.
(53) Ledesma, E. B.; Hoang, J. N.; Nguyen, Q.; Hernandez, V.; Nguyen, M. P.; Batamo, S.; Fortune, C. K. Unimolecular decomposition pathway for the vapor-phase cracking of eugenol, a biomass tar compound. *Energy Fuels* **2013**, *27*, 6839−6846.
(54) Samburova, V.; McDaniel, M.; Campbell, D.; Wolf, M.; Stockwell, W. R.; Khlystov, A. Dominant volatile organic compounds (VOCs) measured at four Cannabis growing facilities: Pilot study results. *J. Air Waste Manage. Assoc.* **2019**, *69*, 1267−1276.
(55) Zhao, Y.; Truhlar, D. G. The M06 suite of density functionals for main group thermochemistry, thermochemical kinetics, noncovalent interactions, excited states, and transition elements: two new functionals and systematic testing of four M06-class functionals and 12 other functionals. *Theor. Chem. Acc.* **2008**, *120*, 215−241.
(56) Weigend, F.; Ahlrichs, R. Balanced basis sets of split valence, triple zeta valence and quadruple zeta valence quality for H to Rn: Design and assessment of accuracy. *Phys. Chem. Chem. Phys.* **2005**, *7*, 3297−3305.
(57) Mardirossian, N.; Head-Gordon, M. ωB97X-V: A 10-parameter, range-separated hybrid, generalized gradient approximation density functional with nonlocal correlation, designed by a survival-of-the-fittest strategy. *Phys. Chem. Chem. Phys.* **2014**, *16*, 9904−9924.
(58) Mardirossian, N.; Head-Gordon, M. How accurate are the minnesota density functionals for noncovalent interactions, isomerization energies, thermochemistry, and narrier heights involving molecules composed of main-group elements? *J. Chem. Theory Comput.* **2016**, *12*, 4303−4325.
(59) Fukui, K. The path of chemical reactions - the IRC approach. *Acc. Chem. Res.* **1981**, *14*, 363−368.
(60) Knizia, G.; Adler, T. B.; Werner, H. J. Simplified CCSD(T)-F12 methods: theory and benchmarks. *J. Chem. Phys.* **2009**, *130*, 054104.
(61) Gordon, M. S.; Schmidt, M. W. Advances in electronic structure theory: GAMESS a decade later. *Theory and Applications of Computational Chemistry*; Elsevier, 2005; pp 1167−1189.
(62) Barca, G. M. J.; Bertoni, C.; Carrington, L.; Datta, D.; De Silva, N.; Deustua, J. E.; Fedorov, D. G.; Gour, J. R.; Gunina, A. O.; Guidez, E.; Harville, T.; Irle, S.; Ivanic, J.; Kowalski, K.; Leang, S. S.; Li, H.; Li, W.; Lutz, J. J.; Magoulas, I.; Mato, J.; Mironov, V.; Nakata, H.; Pham, B. Q.; Piecuch, P.; Poole, D.; Pruitt, S. R.; Rendell, A. P.; Roskop, L. B.; Ruedenberg, K.; Sattasathuchana, T.; Schmidt, M. W.; Shen, J.; Slipchenko, L.; Sosonkina, M.; Sundriyal, V.; Tiwari, A.; Galvez Vallejo, J. L.; Westheimer, B.; Włoch, M.; Xu, P.; Zahariev, F.; Gordon, M. S. Recent developments in the general atomic and molecular electronic structure system. *J. Chem. Phys.* **2020**, *152*, 154102.
(63) Werner, H.-J.; Knowles, P. J.; Knizia, G.; Manby, F. R.; Schütz, M. Molpro: a general-purpose quantum chemistry program package. *Wiley Interdiscip. Rev.: Comput. Mol. Sci.* **2012**, *2*, 242−253.
(64) NIST Mass Spectrometry Data Center, W. E. W., director *"Mass Spectra" in NIST Chemistry WebBook, NIST Standard Reference Database Number 69*; Linstrom, P. J., Mallard, W. G., Eds.; National Institute of Standards and Technology: Gaithersburg MD, 2018; p 20899, (retrieved May 8, 2021).
(65) Moskaleva, L. V.; Lin, M. C. Unimolecular isomerization/decomposition of cyclopentadienyl and related bimolecular reverse process:ab initio MO/statistical theory study. *J. Comput. Chem.* **2000**, *21*, 415−425.
(66) Dubnikova, F.; Lifshitz, A. Ring expansion in methylcyclopentadiene radicals. Quantum chemical and kinetics calculations. *J. Phys. Chem. A* **2002**, *106*, 8173−8183.
(67) Melius, C. F.; Colvin, M. E.; Marinov, N. M.; Pit, W. J.; Senkan, S. M. Reaction mechanisms in aromatic hydrocarbon formation involving the C_5H_5 cyclopentadienyl moiety. *Symp. (Int.) Combust., [Proc.]* **1996**, *26*, 685−692.
(68) Lin, C.-Y.; Lin, M. C. Thermal decomposition of methyl phenyl ether in shock waves: the kinetics of phenoxy radical reactions. *J. Phys. Chem.* **1986**, *90*, 425−431.

https://doi.org/10.1021/acs.energyfuels.1c00858
Energy Fuels 2021, 35, 9994−10008

(69) Bounaceur, R.; Da Costa, I.; Fournet, R.; Billaud, F.; Battin-Leclerc, F. Experimental and modeling study of the oxidation of toluene. *Int. J. Chem. Kinet.* **2005**, *37*, 25−49.
(70) Vasiliou, A. K.; Kim, J. H.; Ormond, T. K.; Piech, K. M.; Urness, K. N.; Scheer, A. M.; Robichaud, D. J.; Mukarakate, C.; Nimlos, M. R.; Daily, J. W.; Guan, Q.; Carstensen, H.-H.; Ellison, G. B. Biomass pyrolysis: thermal decomposition mechanisms of furfural and benzaldehyde. *J. Chem. Phys.* **2013**, *139*, 104310.
(71) da Silva, G.; Bozzelli, J. W. Benzoxyl radical decomposition kinetics: formation of benzaldehyde + H, phenyl + CH_2O, and benzene + HCO. *J. Phys. Chem. A* **2009**, *113*, 6979−6986.
(72) Krasnoukhov, V. S.; Porfiriev, D. P.; Zavershinskiy, I. P.; Azyazov, V. N.; Mebel, A. M. Kinetics of the CH_3 + C_5H_5 reaction: A theoretical study. *J. Phys. Chem. A* **2017**, *121*, 9191−9200.
(73) Moskaleva, L. V.; Mebel, A. M.; Lin, M. C. The CH_3+C_5H_5 reaction: A potential source of benene at high temperatures. *Symp. (Int.) Combust.* **1996**, *26*, 521−526.
(74) He, Y. Z.; Mallard, W. G.; Tsang, W. Kinetics of hydrogen and hydroxyl Radical attack on phenol at high temperatures. *J. Phys. Chem.* **1988**, *92*, 2196−2201.
(75) Mulcahy, M.; Williams, D. Reactions of free radicals with aromatic compounds in the gaseous phase. II. Kinetics of the reaction of methyl radicals with phenol. *Aust. J. Chem.* **1965**, *18*, 20−38.
(76) Johansson, K. O.; Dillstrom, T.; Monti, M.; El Gabaly, F.; Campbell, M. F.; Schrader, P. E.; Popolan-Vaida, D. M.; Richards-Henderson, N. K.; Wilson, K. R.; Violi, A.; Michelsen, H. A. Formation and emission of large furans and oxygenated hydrocarbons from flames. *Proc. Natl. Acad. Sci. U.S.A.* **2016**, *113*, 8374−8379.
(77) Baroncelli, M.; Mao, Q.; Galle, S.; Hansen, N.; Pitsch, H. Role of ring-enlargement reactions in the formation of aromatic hydrocarbons. *Phys. Chem. Chem. Phys.* **2020**, *22*, 4699−4714.
(78) Gueniche, H. A.; Biet, J.; Glaude, P. A.; Fournet, R.; Battin-Leclerc, F. A comparative study of the formation of aromatics in rich methane flames doped by unsaturated compounds. *Fuel* **2009**, *88*, 1388−1393.
(79) Jones, J.; Bacskay, G. B.; Mackie, J. C. Decomposition of the benzyl radical: Quantum chemical and experimental (shock tube) investigations of reaction pathways. *J. Phys. Chem. A* **1997**, *101*, 7105−7113.

https://doi.org/10.1021/acs.energyfuels.1c00858
Energy Fuels 2021, 35, 9994−10008